Perfectly Absorbing Exceptional Points and Chiral Absorbers

William R. Sweeney,^{1,*} Chia Wei Hsu,² Stefan Rotter,³ and A. Douglas Stone^{2,4}

¹Department of Physics, Yale University, New Haven, Connecticut 06520, USA

²Department of Applied Physics, Yale University, New Haven, Connecticut 06520, USA

³Institute for Theoretical Physics, Vienna University of Technology (TU Wien), A-1040 Vienna, Austria

⁴Yale Quantum Institute, Yale University, New Haven, Connecticut 06520, USA

(Received 23 July 2018; published 5 March 2019)

We identify a new kind of physically realizable exceptional point (EP) corresponding to degenerate coherent perfect absorption, in which two purely incoming solutions of the wave operator for electromagnetic or acoustic waves coalesce to a single state. Such non-Hermitian degeneracies can occur at a real-valued frequency without any associated noise or nonlinearity, in contrast to EPs in lasers. The absorption line shape for the eigenchannel near the EP is quartic in frequency around its maximum in any dimension. In general, for the parameters at which an operator EP occurs, the associated scattering matrix does not have an EP. However, in one dimension, when the S matrix does have a perfectly absorbing EP, it takes on a universal one-parameter form with degenerate values for all scattering coefficients. For absorbing disk resonators, these EPs give rise to chiral absorption: perfect absorption for only one sense of rotation of the input wave.

DOI: 10.1103/PhysRevLett.122.093901

Exceptional points (EPs) are generic degeneracies of non-Hermitian systems, where two eigenvalues and eigenvectors of a linear operator coalesce, reducing the size of the space spanned by the eigenbasis [1-5]. EPs arise in open physical systems and are of interest for a number of reasons. For example, they induce chiral behavior under cyclic variation of the parameters of the relevant operator, leading to robust asymmetric state transfer [6,7]. In addition, near an EP a resonant system shows enhanced frequency splitting under small perturbations that may lead to improved sensing [8–10]. EPs can lead to counterintuitive behavior as loss or gain is varied, such as resonance trapping in nuclear and atomic scattering [11,12], enhanced transmission with increasing loss in coupled waveguides [13,14], and suppression of lasing with increasing gain in coupled cavity systems [15,16]. Recently, the work of Wiersig has shown that the chirality associated with EPs can be manifested in disk resonators in the form of chiral lasing [17,18], an effect confirmed in recent experiments by Peng et al. [19].

Two types of EPs have been extensively studied in physics: resonant and scattering. First to be studied were resonant EPs, in which two resonances of an open system coalesce. Resonances are solutions of the wave equation with purely outgoing boundary conditions, typically occurring at complex-valued frequencies, corresponding to poles of the scattering matrix *S*. When parameters in the wave equation are varied, it is possible for two such resonances to coincide (double pole), leading generically to an EP. In unitary systems (e.g., no imaginary part of the index of refraction or potential), resonant EPs can only occur at

complex frequencies (energies) below the real axis, and do not correspond to physical steady-state solutions, although they can still strongly influence the scattering properties for real frequencies [20–22]. By adding gain to an electromagnetic cavity one may bring the resonant EP to a real frequency, corresponding to lasing at threshold. But an amplifying system is not ideal for the study of EPs, due to the large amplified spontaneous emission noise at threshold, and the necessity of including the nonlinearity of the medium to stabilize lasing above threshold.

Scattering EPs are EPs of S and have mainly been studied in systems with balanced loss and gain ($\mathcal{P}\mathcal{T}$ symmetry and related variants), where the scattering eigenchannels make a transition from flux-conserving to amplifying or attenuating propagation [23–25]. In addition, in one-dimensional $\mathcal{P}\mathcal{T}$ -symmetric systems, one can define a permuted S matrix, with a scattering EP at the frequencies at which the system has unidirectional (reflectionless) resonances [24,26,27]. These scattering EPs do not generate the anomalous scattering line shapes or asymmetric state transfer of resonant EPs, nor do they enable the chiral absorption of the absorbing type of resonant EPs identified below. Typical eigenstates of S have both incoming and outgoing components, and hence are not resonances of the system.

Here we study a new kind of EP, the coalescence of two solutions of the wave operator with purely *incoming* boundary conditions, corresponding to perfect absorption. When a *single* such wave solution occurs at a real frequency, it is an example of coherent perfect absorption (CPA) [28–34], a variant and generalization of the concept

of critical coupling [35], in which a particular steady-state incident wave front is completely absorbed. The specific input state is the time reverse of the threshold lasing mode for the same cavity, but with gain replacing loss $[n(\vec{r}) \rightarrow$ $n^*(\vec{r})$]. Achieving CPA typically requires tuning the input frequency and the degree of absorption. With no gain or loss, the frequencies of purely incoming or outgoing states occur in conjugate frequency pairs, $\omega_n \pm i\gamma_n$; the addition of material loss is necessary to move the frequency of a purely incoming state onto the real axis to achieve CPA. Here we study a CPA EP, where two incoming solutions of the wave equation coalesce at a real frequency. The degeneracy of two eigenfrequencies of the incoming wave operator is generically a CPA EP. Exceptions occur for degenerate but decoupled states, e.g., those with different symmetry [31]; these cases will be neglected here. Such absorbing EPs have not been studied before, but should be readily observable with setups previously used to investigate resonant EPs [20,36,37].

The signature of CPA EP in scattering is a quartic behavior (flattening) of the absorption line shape in the perfectly absorbed channel [see Figs. 1(a)–1(f)]; for ordinary CPA it is quadratic. The perfectly absorbed input channel corresponds to an eigenvector of S with eigenvalue zero. To our knowledge, any modification of a line shape associated with an EP has not been previously observed. The quartic behavior generalizes to higher dimensional and/or multichannel, quasi-1D CPA EPs as well, but only in the CPA eigenchannel, and not in the individual scattering coefficients or other eigenchannels [see Fig. 1(d)]. Its origin can be understood as follows: near an ordinary CPA frequency ω_0 , an eigenvalue of S, $\sigma(\omega)$, will pass through zero linearly in the deviation $\delta \equiv \omega - \omega_0$, so that $|\sigma(\omega)|^2 \propto \delta^2$. In the vicinity of the parameter values leading to CPA EP, there are two CPA frequencies near each other $(\omega_0 + \delta_1)$ and $(\omega_0 + \delta_2)$, both belonging to the same eigenvalue $\sigma(\omega)$, whose smooth variation implies $\sigma(\omega) \propto \delta_1 \delta_2$. At CPA EP, $\delta_1 \to \delta_2 \equiv \delta$, and $|\sigma|^2 \propto \delta^4$, which is the quartic absorption line shape. The other conceivable behavior, where distinct S-matrix eigenvalues meet at zero, does not correspond to CPA EP, but rather to an EP of S; the smoothness assumption used above is violated and the line shape is not quartic.

The general properties described above are exemplified by a one-dimensional electromagnetic structure, consisting of two cavities created by a series of three mirrors [see Figs. 1(a)-1(i)]. An EP is realized by coupling the two cavities via a central partially reflecting Bragg mirror and introducing unequal absorption within each cavity. We show three interesting cases. In Figs. 1(a)-1(c), the structure is terminated on the right by a perfect mirror and is accessible only from the left through a partial Bragg mirror, so that S is a scalar, namely, the left reflection amplitude r_L . The absorption is $1-|r_L|^2$. This setup corresponds to the usual critical coupling to a cavity (one-channel CPA),

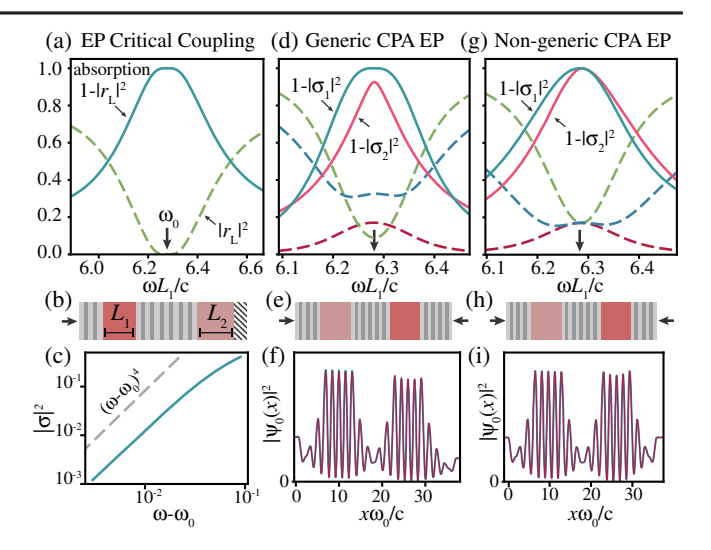


FIG. 1. Scattering from coupled cavity structures at CPA EP for asymmetric (a)-(f) and symmetric (g)-(i) end mirrors. (a),(d), (g) Absorption line shapes of eigenchannels (solid): CPA channel (blue) reaches 100% absorption at the EP frequency ω_0 . In (a),(d) CPA line shape is quartic [see (c)], while in (d) non-CPA channel (red) is quadratic. In (g) we have an EP of S and the line shape is not quartic. Scattering coefficients $|r_L|^2$, $|r_R|^2$, $|t|^2$ are shown as green, blue, and red dashed lines; in (g) they become degenerate at ω_0 , as predicted for an EP of S matrix at zero. (b),(e),(h) Schematics of structures: cavities (red) with lengths L_1 , L_2 , and unequal absorption, emitting to free space through end mirrors. Right mirror is perfect in (b), permeable but unequal to left in (e) and equal to left in (h); parameter values are given in Supplemental Material S1 [38]. (f),(i) CPA EP modes: generic case of unequal coupling (f) yields asymmetric asymptotic values for $|\psi|^2$, implying S not at EP. The CPA mode for nongeneric case of equal coupling (i) has equal asymptotic values, implying that S is at an EP.

except that the cavity is tuned to an EP of the incoming wave operator and hence the absorption line shape is quartic. On the other hand, in Figs. 1(d)–1(f), the Bragg mirrors on the two ends are both permeable and define a two-channel S matrix, characterized by three scattering amplitudes r_L , r_R , t. Here, exciting the absorbing eigenchannel of S requires coherent illumination from both sides with a definite relative intensity and phase [28]. As shown in Fig. 1(d), the quartic absorption line shape is evident for this input state; however, neither the one-sided scattering coefficients $(|r_L|^2, |r_R|^2, |t|^2)$, nor the nonzero eigenchannel exhibit such a flat-top profile.

While Figs. 1(a)-1(f) describe the generic scattering behavior near a CPA EP, there is a novel and interesting nongeneric case, exemplified by Figs. 1(g)-1(i), which can be realized in the same type of geometry, and does *not* show the generic quartic line shape, but has different and striking scattering properties. This is a case where CPA EP and an EP of the *S* matrix approximately coincide. Hence we now discuss the relationship between exceptional behavior of the wave operator and of *S*.

Every eigenstate of the wave operator with incoming boundary conditions also corresponds to an eigenvector of *S* with eigenvalue zero. However, the coalescence of two incoming states does *not* simultaneously generate an EP of *S*, as we now prove.

For simplicity, consider an arbitrary one-dimensional cavity described by the Helmholtz equation:

$$\{\nabla^2 + \varepsilon(x)k_i^2\}\psi_i(x) = 0, \tag{1}$$

where $\varepsilon(x)$ is the dielectric function of the medium, $k_j = \omega_j/c$, and ω_j are the discrete complex eigenfrequencies with purely incoming boundary conditions. Consider two eigenfrequencies, ω_1 , ω_2 , initially with different values and linearly independent solutions, $\psi_1(x)$, $\psi_2(x)$. Further assume that tuning $\varepsilon(x)$ causes these two solutions to coalesce at ω_0 : ψ_1 , $\psi_2 \to \psi_0$. By using the wave equation (1) and taking the limit $\omega_1 \to \omega_2 \equiv \omega_0$, one can derive the identity (see Supplemental Material S2 [38])

$$-2i\omega_0 \int_{\text{cav}} dx \psi_0(x) \varepsilon(x) \psi_0(x) = c_0 \hat{s}_0 \cdot \hat{s}_0, \qquad (2)$$

where \hat{s}_0 is the normalized eigenvector of the S matrix corresponding to ψ_0 (i.e., with eigenvalue zero), and c_0 is a system-specific constant. The integral on the left-hand side (LHS) of Eq. (2) in general does not vanish. Solutions of the wave equation with either purely incoming or outgoing boundary conditions do not satisfy any simple biorthogonality relation over the scattering region [2,43]. Hence at an EP of the incoming wave operator, integrals of this type are nonzero (see Supplemental Material S2 for discussion of EP self-orthogonality in open systems [38]). On the other hand, the right-hand side of Eq. (2) is proportional to the biorthogonal norm of the eigenvector of the symmetric S matrix with eigenvalue zero; as such it vanishes if and only if S is also at an EP [44]. A nonvanishing LHS implies that CPA EP does not in general correspond to an EP of S; indeed for the generic case shown in Figs. 1(d)-1(f) the S matrix has a second eigenvector which is not perfectly absorbed at CPA EP (red solid line), and hence has nonzero scattering. This proof generalizes to higher dimensional scattering geometries using Green's theorem.

Conversely, one can find scattering geometries and structures for which an EP of *S* can occur for eigenvalue equal to zero; however this does *not* in general imply CPA EP. The EP of *S* at zero is a specific case of a scattering EP of the type mentioned above [23–25]; we discuss its implications briefly below. The general case of scattering EPs will be discussed elsewhere [45].

A 2×2 *S* matrix with zero eigenvalue, tuned to an EP at frequency ω_0 , satisfies $r_L(\omega_0) = -r_R(\omega_0) = \pm it(\omega_0)$. Hence all the scattering coefficients are equal at ω_0 :

$$|r_L(\omega_0)|^2 = |r_R(\omega_0)|^2 = |t(\omega_0)|^2.$$
 (3)

This signature of an EP of S at zero can thus be observed simply with standard one-sided reflection and transmission measurements. The scattering behavior of the structure shown in Figs. 1(g)-1(i) shows precisely the triple degeneracy of the scattering coefficients characteristic of an EP of S at zero [Eq. (3)]. This is initially surprising, since its parameters were chosen to be at CPA EP, not at an EP of S. The structure differs from that of Fig. 1(e) only by the imposition of identical Bragg end mirrors.

To understand why for this structure CPA EP and an EP of S coincide we use temporal-coupled mode theory (TCMT) [46], which provides an analytic but approximate relationship between the eigenfrequencies of the wave operator and the S matrix. Within TCMT one can show (Supplemental Material S3 [38]) that when the two cavities have equal out-coupling rates, CPA EP does imply a simultaneous EP of the S matrix, but not when the cavities have unequal out-coupling rates. Thus, essentially the same experimental setup can test the properties of these two different types of absorbing EPs. If the TCMT theory were exact, the two eigenvalues of S would coincide precisely at ω_0 and would not be analytic there, leading to a complicated, nonquartic behavior near CPA. Because of the approximate nature of TCMT, we find a slight displacement of the EP of S from CPA EP, not visible in the results of Fig. 1(g).

Returning to generic CPA EP, we now explore higher dimensional structures, both in free space and guided wave geometries. For the case of resonant EPs, there has been extensive study of perturbed and deformed disk resonators in 2D, for which the EP of whispering gallery modes (WGMs) directly implies a spatially chiral solution, corresponding to either clockwise (CW) or counterclockwise (CCW) circulations of waves in the disk [17,18,47]. These strongly chiral resonances have been probed experimentally through asymmetric backscattering and chiral laser emission [19]. We now show that CPA EP in such a system will lead to chiral absorption: perfect absorption for, e.g., CCW input, and substantial backscattering for CW. We note that standard CPA in disk and sphere resonators has been studied previously [30,34].

We first consider an example of chiral absorption in free space, adapting the Wiersig model of a dielectric disk perturbed by two point scatterers [17], with parameters chosen to realize an absorbing EP at a real frequency (see Supplemental Material S1 [38]). The perturbation from the first point scatterer splits the degenerate WGMs at angular momenta $m=\pm q$ into two standing-wave resonances, and fine-tuning the perturbation due to the second scatterer brings these two resonances back to degeneracy, forming an EP with CCW chirality at a complex frequency. Finally, introducing a critical degree of absorption brings the absorbing EP to a real frequency. As the scatterers break the rotational symmetry of the structure, the CPA EP input involves a coherent superposition of many angular momenta

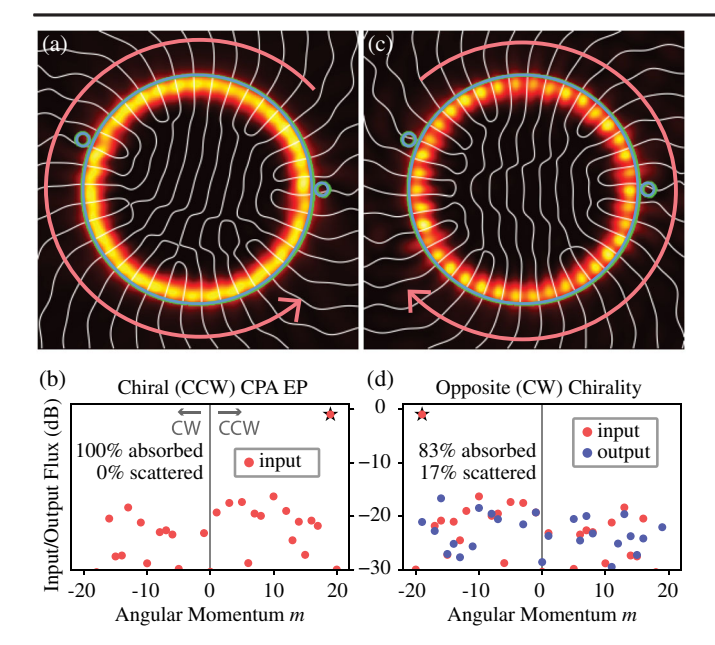


FIG. 2. Chiral CPA EP of WGMs of absorbing microdisk perturbed by point scatterers. (a) CCW incident CPA EP mode. Intensity plotted as color scale, curves of constant phase (white), disk boundary and scatterers (blue). Curvature of phase fronts shows sense of rotation, denoted by arrow. Uniform intensity along rim indicates running wave in disk. (b) Input fluxes carried in each angular momentum channel for CPA EP (CCW) input. Dominant channel (denoted by star) carries 80% of flux; CPA input is > 99.9% absorbed. (c) Total field (incident and scattered) for reverse chirality input. Internal intensity shows standing wave oscillations due to presence of backscattering. (d) As in (b), input fluxes (red), output (blue), for CW input. Here we find ~1% scattering across many channels, giving a total of 17% scattered flux (83% absorption).

other than $\pm q$, although at significantly weaker amplitude. For the example shown in Fig. 2, the perfectly absorbed state has 80% of its incident flux at q=19, with the remaining 20% distributed across both CW and CCW at other m's. We test the chirality of absorption by exciting the disk with the corresponding CW input by exchanging $c_m \leftrightarrow (-)^m c_{-m}$ in the superposition; whereas the original state is 100% absorbed, the opposite chirality is only 83% absorbed. Moreover, if we approximate the CPA input state by just its dominant component (m=19), both chiralities are equally absorbed (81%).

The wave front of the above free-space chiral CPA can be readily generated for acoustic waves, but an optical implementation may be challenging. Therefore, we next consider chiral CPA EPs that are coupled in through a waveguide or fiber (see Fig. 3). To reach CPA with a waveguide-only input, the free-space scattering loss rate should be much smaller than the waveguide coupling rate. Thus, using point scatterers as tuning perturbations is undesirable, as they introduce additional scattering to free space. Therefore, instead of point scatterers, we introduce an azimuthally varying grating on the real and imaginary

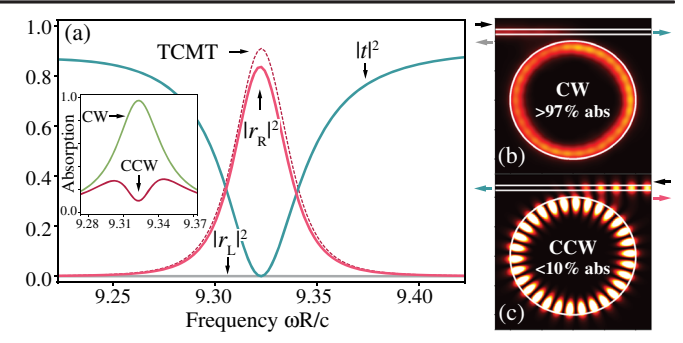


FIG. 3. Chiral absorption from CPA EP waveguide-microdisk system. (a) Reflection $|r_L|^2$ (gray), $|r_R|^2$ (red solid), and transmission $|t|^2$ (blue) for disk with complex index azimuthal grating, tuned to CPA EP. TCMT prediction [Eq. (4)] for r_R in dashed red. Inset: one-sided absorption spectrum for left illumination (green) and right (red). (b) Intensity of total field (incident & scattered) for left illumination, corresponding to CPA EP. (c) Same as (b) but for right illumination. Note standing wave of (c) vs running wave of (b) indicates strong coupling between CW and CCW modes only for right incidence, causing chiral absorption.

parts of the refractive index to promote the non-Hermitian asymmetric coupling via absorption loss. The system is well modeled by TCMT, taking into account only the two single-mode running wave solutions in the fiber and the CW and CCW angular momentum states in the disk, coupled via the grating. This configuration is similar to those used to study $\mathcal{P}T$ -symmetry breaking and unidirectional invisibility in Refs. [26,37,48–51], but here we do not introduce any gain into the grating, only variable loss and a varying real part of the index, with no $\mathcal{P}T$ -like discrete symmetries (see Supplemental Material S4B [38]).

The dielectric grating in Fig. 3 has a separable form $\delta \varepsilon = \rho(r)\tau(\theta)\varepsilon_0$ and couples WGMs with angular momenta $m = \pm q$ via azimuthal Fourier components $au_{\pm 2q}$, where $au(heta) = \sum_n au_n e^{in heta}$ ($arepsilon_0$ is the dielectric function of the disk without the grating). To achieve EP, one of the $\pm 2q$ components must vanish while the other remains finite (see Supplemental Material S4A [38]), which can only occur with a complex index grating. With the grating choice in Fig. 3, $\tau_{-2a} = 0$, implying that the right propagating (CW) input at CPA EP will be strongly absorbed with negligible reflection, while $\tau_{2q} \neq 0$ will cause partial reflection of the left propagating (CCW) input. Experimentally relevant gratings are piecewise constant, and in the simplest case have real and imaginary parts with the same angular width ϕ and periodicity $2\pi/P$, and an angular offset χ between them. In this case, we show in the Supplementary Material (S4B) [38] that an EP for WGMs with $m = \pm q$ is achieved when the real and the imaginary gratings have the same modulation magnitude, offset $\chi = (M - 1/4)\pi/q$, and where P divides 2q $(M, P \in \mathbb{Z})$. Critically coupling the waveguide to the disk yields the desired CPA EP, with $r_L(\delta) = 0$ and

$$t(\delta) = \frac{\delta}{\delta + i\Gamma}, \qquad |r_R(\delta)|^2 = \left(\frac{\sin q\phi}{q\phi}\right)^2 \frac{1}{(1 + \delta^2/\Gamma^2)^2},$$
(4)

where $\delta = \omega - \omega_0$ is the detuning from the CPA EP frequency, and Γ is the HWHM of the dip in $|t^2|$. Note that to maximize reflection from the right (and minimize absorption), thinner lines of the grating are better, as this allows the standing wave to align its nodes with the narrower absorbing regions. The reflection line shape is a squared Lorentzian [39], while the transmission line shape remains unaffected (Supplemental Material S4A [38]). As expected, the eigenchannel of S (which is two-sided except at ω_0) exhibits a quartic line shape (not shown).

If we turn now to the results of the exact finite-difference frequency-domain numerical calculations (Fig. 3), we see that indeed the absorption in this geometry is strongly chiral, being > 97% when the disk resonance is excited from the left (CW excitation), but < 10% when it is excited from the right (CCW excitation), the difference appearing predominantly as backscattering into the waveguide as expected, and in good agreement with the TCMT model. Note that the 2.7% of the input which is not absorbed for the CW excitation is removed by free space radiation and the CW reflection is truly negligible (Supplemental Material S5 [38]).

We gratefully acknowledge useful discussions with Lan Yang, Changqing Wang, Mengzhen Zheng, and Liang Jiang. A. D. S. acknowledges support under NSF Grant No. DMR-1743235. S. R. acknowledges support by the European Commission under Project No. NHQWAVE (MSCA-RISE 691209).

- *william.sweeney@yale.edu
- [1] T. Kato, *Perturbation Theory for Linear Operators* (Springer-Verlag, Berlin, Heidelberg, 1995).
- [2] N. Moiseyev, *Non-Hermitian Quantum Mechanics* (Cambridge University Press, Cambridge, England, 2011).
- [3] W. D. Heiss, J. Phys. A 45, 444016 (2012).
- [4] L. Feng, R. El-Ganainy, and L. Ge, Nat. Photonics **11**, 752 (2017).
- [5] R. El-Ganainy, K. G. Makris, M. Khajavikhan, Z. H. Musslimani, S. Rotter, and D. N. Christodoulides, Nat. Phys. 14, 11 (2018).
- [6] J. Doppler, A. A. Mailybaev, J. Böhm, U. Kuhl, A. Girschik, F. Libisch, T. J. Milburn, P. Rabl, N. Moiseyev, and S. Rotter, Nature (London) 537, 76 (2016).
- [7] H. Xu, D. Mason, L. Jiang, and J. G. E. Harris, Nature (London) 537, 80 (2016).
- [8] W. Chen, Ś. K. Özdemir, G. Zhao, J. Wiersig, and L. Yang, Nature (London) 548, 192 (2017).
- [9] H. Hodaei, A. U. Hassan, S. Wittek, H. Garcia-Gracia, R. El-Ganainy, D. N. Christodoulides, and M. Khajavikhan, Nature (London) 548, 187 (2017).

- [10] M. Zhang, W. R. Sweeney, C. W. Hsu, L. Yang, A. D. Stone, and L. Jiang, arXiv:1805.12001.
- [11] E. Persson, I. Rotter, H. J. Stöckmann, and M. Barth, Phys. Rev. Lett. 85, 2478 (2000).
- [12] I. Rotter, J. Phys. A 42, 153001 (2009).
- [13] A. Guo, G. J. Salamo, D. Duchesne, R. Morandotti, M. Volatier-Ravat, V. Aimez, G. A. Siviloglou, and D. N. Christodoulides, Phys. Rev. Lett. 103, 093902 (2009).
- [14] C. E. Ruter, K. G. Makris, R. El-Ganainy, D. N. Christodoulides, M. Segev, and D. Kip, Nat. Phys. 6, 192 (2010).
- [15] M. Liertzer, L. Ge, A. Cerjan, A. D. Stone, H. E. Türeci, and S. Rotter, Phys. Rev. Lett. 108, 173901 (2012).
- [16] M. Brandstetter, M. Liertzer, C. Deutsch, P. Klang, J. Schöberl, H. E. Türeci, G. Strasser, K. Unterrainer, and S. Rotter, Nat. Commun. 5, 4034 (2014).
- [17] J. Wiersig, Phys. Rev. A 84, 063828 (2011).
- [18] J. Wiersig, Phys. Rev. A 89, 012119 (2014).
- [19] B. Peng, Ś. K. Özdemir, M. Liertzer, W. Chen, J. Kramer, H. Yılmaz, J. Wiersig, S. Rotter, and L. Yang, Proc. Natl. Acad. Sci. U.S.A. 113, 6845 (2016).
- [20] B. Peng, Ś. K. Özdemir, F. Lei, F. Monifi, M. Gianfreda, G. L. Long, S. Fan, F. Nori, C. M. Bender, and L. Yang, Nat. Phys. 10, 394 (2014).
- [21] B. Zhen, C. W. Hsu, Y. Igarashi, L. Lu, I. Kaminer, A. Pick, S.-L. Chua, J. D. Joannopoulos, and M. Soljačić, Nature (London) 525, 354 (2015).
- [22] H. Zhou, C. Peng, Y. Yoon, C. W. Hsu, K. A. Nelson, L. Fu, J. D. Joannopoulos, M. Soljačić, and B. Zhen, Science 359, 1009 (2018).
- [23] Y. D. Chong, L. Ge, and A. D. Stone, Phys. Rev. Lett. 106, 093902 (2011).
- [24] L. Ge, Y. D. Chong, and A. D. Stone, Phys. Rev. A 85, 023802 (2012).
- [25] P. Ambichl, K. G. Makris, L. Ge, Y. Chong, A. D. Stone, and S. Rotter, Phys. Rev. X 3, 041030 (2013).
- [26] Z. Lin, H. Ramezani, T. Eichelkraut, T. Kottos, H. Cao, and D. N. Christodoulides, Phys. Rev. Lett. 106, 213901 (2011).
- [27] Y. Huang, Y. Shen, C. Min, S. Fan, and G. Veronis, Nanophotonics **6**, 977 (2017).
- [28] Y. D. Chong, L. Ge, H. Cao, and A. D. Stone, Phys. Rev. Lett. 105, 053901 (2010).
- [29] W. Wan, Y. Chong, L. Ge, H. Noh, A. D. Stone, and H. Cao, Science 331, 889 (2011).
- [30] H. Noh, Y. Chong, A. D. Stone, and H. Cao, Phys. Rev. Lett. 108, 186805 (2012).
- [31] J. R. Piper, V. Liu, and S. Fan, Appl. Phys. Lett. 104, 251110 (2014).
- [32] B. Zhen, C. W. Hsu, H. Zhou, J. D. Joannopoulos, M. Soljačić, O. D. Miller, and S. G. Johnson, Optica 3, 1079 (2016).
- [33] H. Zhao, W. S. Fegadolli, J. Yu, Z. Zhang, L. Ge, A. Scherer, and L. Feng, Phys. Rev. Lett. **117**, 193901 (2016).
- [34] D. G. Baranov, A. Krasnok, T. Shegai, A. Alù, and Y. Chong, Nat. Rev. Mater. 2, 17064 (2017).
- [35] A. Yariv, Electron. Lett. **36**, 321 (2000).
- [36] L. Chang, X. Jiang, S. Hua, C. Yang, J. Wen, L. Jiang, G. Li, G. Wang, and M. Xiao, Nat. Photonics 8, 524 (2014).
- [37] P. Miao, Z. Zhang, J. Sun, W. Walasik, S. Longhi, N. M. Litchinitser, and L. Feng, Science 353, 464 (2016).

- [38] See Supplemental Material at http://link.aps.org/supplemental/10.1103/PhysRevLett.122.093901 for details of the calculations shown in Fig. 1, for a derivation of Eq. (2) and discussion of self-orthogonality, and for the calculation of scattering amplitudes cited in Eq. (4). This includes Refs. [2,39–42].
- [39] A. Pick, B. Zhen, O. D. Miller, C. W. Hsu, F. Hernandez, A. W. Rodriguez, M. Soljačić, and S. G. Johnson, Opt. Express 25, 12325 (2017).
- [40] Ya. B. Zel'dovich, Sov. Phys. JETP 12, 542 (1961).
- [41] H. M. Lai, P. T. Leung, K. Young, P. W. Barber, and S. C. Hill, Phys. Rev. A 41, 5187 (1990).
- [42] Optical Processes in Microcavities, edited by R. K. Chang and A. J. Campillo (World Scientific, Singapore, 1996).
- [43] P. T. Leung, S. Y. Liu, and K. Young, Phys. Rev. A 49, 3057 (1994).

- [44] L. N. Trefethen and M. Embree, *Spectra and Pseudospectra* (Princeton University, Princeton, NJ, 2005).
- [45] W. R. Sweeney, C. W. Hsu, and A. D. Stone (to be published).
- [46] H. A. Haus, *Waves and Fields in Optoelectronics* (Prentice-Hall, Englewood Cliffs, NJ, 1984).
- [47] H. Cao and J. Wiersig, Rev. Mod. Phys. 87, 61 (2015).
- [48] A. Regensburger, C. Bersch, M.-A. Miri, G. Onishchukov, D. N. Christodoulides, and U. Peschel, Nature (London) 488, 167 (2012).
- [49] L. Feng, Y.-L. Xu, W. S. Fegadolli, M.-H. Lu, J. E. B. Oliveira, V. R. Almeida, Y.-F. Chen, and A. Scherer, Nat. Mater. 12, 108 (2013).
- [50] S. Longhi and L. Feng, Opt. Lett. 39, 5026 (2014).
- [51] L. Feng, Z. J. Wong, R.-M. Ma, Y. Wang, and X. Zhang, Science 346, 972 (2014).